Available online at www.sciencedirect.com
SCIENCE DIRECT
Polymer 46 (2005) 2266–2275
polymer
www.elsevier.com/locate/polymer

A new kinetic model for interdiffusion at semicrystalline polymer interfaces

Chieh-Tsung Lo, Balaji Narasimhan*

Department of Chemical Engineering, Iowa State University, 2035 Sweeney Hall, Ames, IA 50011-2230, USA

Received 27 August 2004; received in revised form 6 December 2004; accepted 12 January 2005

Abstract

A kinetic model has been developed to describe the behavior of semicrystalline polymer interfaces. In these systems, the competition between interdiffusion and crystallization drives the overall transport. The crystallization rate is based on the Avrami equation, in which the Avrami exponent and the crystallization rate constant as a function of temperature and blend composition are determined by in situ optical microscopy and differential scanning calorimetry. The mutual diffusion coefficient is obtained by using the fast mode theory. The predicted density profiles as a function of position are used to extract the interfacial widths, which are affected by molecular weight, equilibrium degree of crystallinity, and temperature. At low temperatures, the crystallization rate is fast, and the crystals present near the interface hinder the interdiffusion, causing the interfacial width to be small. At high temperatures, the crystallization is much slower, and interdiffusion dominates crystallization. The model predictions are compared with interfacial behavior observed by transmission electron microscopy and small angle X-ray scattering in a system composed of polyethylene and isotactic polypropylene and the agreement with the experiments is satisfactory.

Keywords: Semicrystalline polymer interface; Kinetic model; Interdiffusion

1. Introduction

Polymer interfaces are scientifically exciting and have industrial relevance due to extensive applications involving artificial organs, aircraft bodies, and electronic materials [1]. A detailed understanding of polymer interfaces is necessary to control processing and design materials with tailored properties. Polymer interfaces, particularly in amorphous polymer systems, have been widely studied using both simulation and experiment [2–15], and relationships have been derived between molecular properties (entanglements, architecture) and interfacial properties (interfacial width, fracture strength). For example, it has been proposed that the interfacial strength in amorphous polymer systems increases with interfacial width [1,16–18] when the molecular weight exceeds the critical entanglement molecular weight (M_c).

Based on their interfacial behavior, polymer interfaces can be classified as symmetric, asymmetric, and semicrystalline [1]. In symmetric interfaces, both polymers are identical, and the interfacial behavior is solely controlled by self-diffusion, which affects the interfacial width. Wool et al. [1,19] derived a scaling law for the interfacial thickness (w) using the minor chain reptation model [20]. At times less than the reptation time, T_r, interdiffusion is obstructed by the neighboring chains, and the interfacial width as a function of time (t) is given as follows.

$$w = 1.6\, R_g \left(\frac{t}{T_r}\right)^{1/4} \tag{1}$$

here R_g is the radius of gyration. As $t > T_r$, the minor chains escape from the barrier, and are free to move across the interface. At this stage, the interfacial width depends on the self-diffusion coefficient, D_s ($w \sim 2(D_s t)^{1/2}$), and Eq. (1) is replaced by

$$w = 1.6\, R_g \left(\frac{t}{T_r}\right)^{1/2} \tag{2}$$

In asymmetric polymer interfaces, the interfacial width is

* Corresponding author. Tel.: +1 515 294 8019; fax: +1 515 294 2689.
E-mail address: nbalaji@iastate.edu (B. Narasimhan).

0032-3861/$ - see front matter © 2005 Elsevier Ltd. All rights reserved.
doi:10.1016/j.polymer.2005.01.036

strongly dependent on the compatibility of the two components. Helfand et al. [21–23] used a self-consistent field theory to predict the behavior of immiscible polymer interfaces. The theory is based on the balance between immiscibility, which forces the two materials apart, and incompressibility, which resists the separation. In this theory, the interfacial width can be expressed as

$$w_\infty = \frac{2c_s}{\sqrt{6\chi}} \tag{3}$$

here, w_∞ is the interfacial width (for polymers of infinite molecular weight), c_s is the segment length, and χ is the segmental interaction parameter. Anastasiadis et al. [24] expanded on this idea by utilizing the molecular weight dependence of the interfacial tension, which is related to the interfacial width. They found that interfacial tension increases with molecular weight, while the interfacial width decreases with molecular weight. Broseta et al. [25] proposed a mean field model to predict the interfacial width of asymmetric polymer interfaces with finite molecular weight (see Eq. (4)).

$$w = w_\infty \left[1 + \ln 2\left(\frac{1}{\chi N_A} + \frac{1}{\chi N_B}\right)\right] \tag{4}$$

here N_i is the degree of polymerization of component i. The correction due to finite molecular weight is based on entropic concerns, and the interfacial width becomes broader. It is important to note that Eq. (4) is valid only when the volume fraction of either component is $\sim$0.5. Broseta et al. [25] also studied the effect of polydispersity on interfacial behavior by assuming a bimodal molecular weight distribution. They found that small chains favor accumulation at the interface due to the small interfacial tension. When the polymer chains on either side of the interface are very long, these effects can be ignored. Chaturvedi et al. [26] also proposed a mean field model for the χ dependence of interfacial width in incompatible systems.

$$w = \frac{c_s\sqrt{2}}{3\chi_c}\left(\frac{\chi}{\chi_c} - 1\right)^{-1/2} \tag{5}$$

here χ_c is the χ value at the critical temperature. The interfacial width predicted by their mean field model is in quantitative agreement with that measured by ion-beam methods based on nuclear reaction analysis [26].

Stamm and Schubert [27] compared the predictions of various interfacial width models with interfacial widths measured by several experimental techniques, such as neutron and X-ray reflectivity, interfacial tension measurements, and nuclear reaction analysis. They concluded that the theoretical interfacial widths are always smaller than experimentally measured interfacial width due to some ignored contributions in the theories, such as concentration fluctuations, chain end effects, distorted chain conformation, polydispersity, and initial roughness.

In contrast, semicrystalline polymer interfaces have not received as much attention, both theoretically and experimentally. In semicrystalline polymer systems, in addition to interdiffusion and miscibility, crystallization affects the interfacial behavior. Several researchers have shown that interfacial behavior depends on the location of nucleation [28,29]. At low temperature, nucleation occurs at the interface, which acts as a barrier for interdiffusion, and the interfacial width is small. At high temperature, nucleation is far away from the interface, and interdiffusion dominates crystallization, leading to a large interfacial width. Moreover, volume contraction due to the crystallization may provide free volume for interdiffusion [30,31].

Kumar and Yoon [32–34] predicted the interfacial width of compatible semicrystalline polymer systems by a lattice model. By an assumption that crystallization causes phase separation, they found that the interfacial width is strongly dependent on the segmental interaction parameter, and the relationship is shown in Eq. (6)

$$w \propto \frac{3}{(-\chi)^{1/2}} \tag{6}$$

This relationship is similar to Eq. (3) for amorphous polymer systems, but both equations can only be used in the limit of compatibility of components.

The focus of this paper is the development of a kinetic model to understand the behavior of semicrystalline polymer interfaces in which crystallization, miscibility and interdiffusion are taken into account. The overall goal is to understand the effect of the competition between crystallization and interdiffusion on interfacial behavior, and identify how molecular properties influence interfacial performance in these systems. The semicrystalline polymer system of interest is made of isotactic polypropylene (iPP) and linear low-density polyethylene (PE). Since this study is focused on the effects of interdiffusion and crystallization on interfacial behavior, annealing temperatures between the melting temperatures of the two polymers were chosen so that only iPP crystallizes during processing.

2. Theory

2.1. Crystallization

The kinetics of isothermal crystallization for a homopolymer is expressed by the Avrami equation [35–37]

$$\phi_c = 1 - \exp(-kt^m) \tag{7}$$

here, ϕ_c is the volume fraction of crystals, k is the crystallization rate constant, and m is the Avrami exponent. The Avrami parameters, m and k, can be obtained by plotting $\ln(-\ln(1-\phi_c))$ versus $\ln t$ at isothermal crystallization conditions. It has been proposed that in the iPP/PE blend system, PE dilutes the iPP nucleation [38–40], and

that the viscosity of PE slows down the iPP chain mobility toward the crystallization front [39]. Thus as the PE fraction in the blend increases, the iPP crystallization rate decreases.

During crystallization, nucleation occurs, followed by spherulite growth. Both processes are temperature dependent. A general expression for crystal growth proposed by Lauritzen and Hoffman [41] is used.

$$G^* = G_o{}^* \exp\left(-\frac{U^*}{R(T_c - T_\infty)}\right)\exp\left(-\frac{K_g}{fT_c\Delta T}\right) \tag{8}$$

here, G^* is the crystal growth rate, $G_o{}^*$ is a constant, U^* is the activation energy for polymer diffusion, R is the gas constant, T_c is the crystallization (or annealing) temperature, T_∞ is the reference temperature, K_g is the nucleation rate constant, ΔT is the degree of supercooling ($=T_m^o - T_c$, where T_m^o is the melting temperature of an infinitely thick crystal), and $f = 2T_c/(T_c + T_m^o)$. In the Lauritzen–Hoffman theory, at the beginning of crystal growth, the chains diffuse to the crystallization front, and create secondary nuclei, which spread over the substrate or crystal surface, and complete a new layer of lamellae. The parameter K_g in Eq. (8) can be expressed as

$$K_g = \frac{jb_o\sigma\sigma_e T_m^o}{k_B\Delta h_f} \tag{9}$$

Here, b_o is the width of the folded chains, σ and σ_e are the fold surface and lateral surface free energy respectively, k_B is the Boltzmann constant, Δh_f is the heat of fusion, and j is a constant based on the three regimes of crystallization kinetics, which depends on the degree of supercooling [41–43]. In the blend, due to the dilution of the nucleation and the change in viscosity, the parameters U^* and K_g in Eq. (8) are affected.

Based on the exponential expression for crystal growth (Eq. (8)), we assume the temperature and composition dependence of k as

$$k = a\exp\left(\frac{c}{R(T - T_\infty)}\right)[\exp(b\phi_{iPP}) - 1] \tag{10}$$

here, T is the annealing temperature, ϕ_{iPP} is the volume fraction of iPP in the blend, and a, b, and c are constants. The composition dependence of k has been chosen to account for the barrier to crystallization due to the dilution. Thus, when ϕ_{iPP} in the blend is zero, which means that there is only amorphous PE in the system, k is zero, and no crystallization occurs.

2.2. Interdiffusion

In asymmetric polymer interfaces, both polymers are dissimilar, and the compatibility of the two materials affects the interdiffusion. The interdiffusion coefficient, or the mutual diffusion coefficient, D, of an asymmetric polymer system can be deduced by relating the Flory–Huggins equation [44] with the chemical potential gradient, and D is given by [45,46]

$$D = 2\phi_A\phi_B D_T(\chi_s - \chi) \tag{11}$$

here, ϕ_i is the volume fraction of component i, D_T is the transport coefficient, which is composition dependent, and χ_s is the value of χ at the spinodal, which is given by

$$\chi_s = \frac{1}{2}\left(\frac{1}{N_A\phi_A} + \frac{1}{N_B\phi_B}\right) \tag{12}$$

the expression for D_T is based on the relative mobility of the two components. In the slow mode theory [46], the slower moving component dominates the mutual diffusion coefficient, and Eq. (11) is given by

$$D = \left(\frac{N_A D_A N_B D_B}{N_A D_A\phi_A + N_B D_B\phi_B}\right) \times \left(\frac{\phi_B}{N_A} + \frac{\phi_A}{N_B} - 2\phi_A\phi_B\chi\right) \tag{13}$$

here, D_A and D_B are the self-diffusion coefficients. In contrast, the fast mode theory [2,45] assumes the mutual diffusion coefficient is dominated by the faster moving component, and is given by

$$D = (\phi_B N_A D_A + \phi_A N_B D_B) \times \left(\frac{\phi_B}{N_A} + \frac{\phi_A}{N_B} - 2\phi_A\phi_B\chi\right) \tag{14}$$

It has been observed that many asymmetric amorphous polymer systems exhibit interdiffusion behavior consistent with the fast mode theory [2,15,47–52]. The fast mode theory has also been used to model interdiffusion in a polymer system in which one component crystallizes [53].

The self-diffusion coefficients, D_A and D_B, both depend on molecular weight and temperature [54]. In general, for polymers with molecular weights exceeding the entanglement molecular weight, the diffusion coefficient depends on molecular weight (M) as shown in Eq. (15).

$$D_i \propto \frac{1}{M^2} \tag{15}$$

In our model, the self-diffusion coefficients of iPP (D_{iPP}) and PE (D_{PE}) are extracted from the data published by Gell et al. [55] and Tirrell [54], respectively.

$$D_{iPP} = 2.1 \times 10^{-4}\ M^{-2}\ (cm^2/s) \tag{16}$$

$$D_{PE} = 9.0 \times 10^{-1}\ M^{-2}\ (cm^2/s) \tag{17}$$

In Eqs. (16) and (17), D_{iPP} and D_{PE} were measured at 50 °C and 176 °C, respectively. Since the diffusion coefficients are a function of temperature, the Arrhenius expression is used to model the temperature dependence of D_{iPP} and D_{PE} [56] as shown below.

$$D_i \propto \exp\left(\frac{-\Delta E_i}{RT}\right) \tag{18}$$

here, ΔE_i is the activation energy of component i. The activation energy of PE and iPP are reported as 22.3 kJ/mol [54] and 39 kJ/mol [57] respectively.

2.3. Kinetics of semicrystalline polymer interdiffusion at interfaces

The model describes the kinetics of diffusion of semicrystalline polymers across an interface. In this model, one of the polymers is amorphous, and the other is semicrystalline. The bilayer thickness is L. Initially, the two polymers are separated into two domains (each of thickness 0.5L), and the degree of crystallinity of iPP is zero, indicating that the crystals are eliminated by annealing above the melting temperature prior to any interdiffusion. This is a one dimensional, fixed boundary problem, and the three components in the system are the volume fractions of amorphous PE (v_{1a}), amorphous iPP (v_{2a}) and crystalline iPP (v_{2c}).

The expression for the rate of change of crystalline iPP is given by

$$\frac{\partial v_{2c}}{\partial t} = mkt^{m-1}\exp(-kt^m) \tag{19}$$

This equation directly arises from the Avrami equation (see Eq. (7)) and expresses the crystallization rate of iPP. The rate of change of the amorphous iPP is controlled by two terms: an interdiffusion term and a phase change (from amorphous to crystalline) term. The mutual diffusion coefficient is based on the fast mode theory as shown in Eq. (14). We have characterized the phase behavior of the iPP/PE system by small angle X-ray scattering [58] and extracted the temperature dependence of χ as shown below.

$$\chi = -0.0367 + \frac{16.01}{T} \tag{20}$$

thus, the rate of change of amorphous iPP can be written as

$$\frac{\partial v_{2a}}{\partial t} = \frac{\partial}{\partial x}\left(D\frac{\partial v_{2a}}{\partial x}\right) - \frac{\partial v_{2c}}{\partial t} \tag{21}$$

The interfacial behavior is affected by both interdiffusion and crystallization. Thus, the volume fraction of amorphous iPP increases due to the interdiffusion process and simultaneously decreases because of the formation of iPP crystals. Eq. (21) models this competition. The interdiffusion of amorphous iPP is modeled using a Fickian equation with a composition-dependent mutual diffusion coefficient, and the decrease of amorphous of iPP is simply taken from Eq. (19). Initially, iPP and PE are amorphous and divided into two separated regions. Therefore, the initial conditions are as follows:

$$\text{At } t = 0,\ 0 < x \le \frac{L}{2},\ v_{1a} = 1,\ v_{2a} = v_{2c} = 0 \tag{22}$$

$$\frac{L}{2} < x \le L,\ v_{2a} = 1,\ v_{2c} = 0,\ v_{1a} = 0 \tag{23}$$

At the outer boundary, no flux boundary conditions are imposed.

$$\text{At } x = 0 \text{ and } x = L,\ \frac{\partial v_{1a}}{\partial x} = \frac{\partial v_{2a}}{\partial x} = 0 \tag{24}$$

This completes the formulation of the problem, which contains a moving interface. The distance, x, is then normalized by the bilayer thickness.

$$\xi = \frac{x}{L} \tag{25}$$

thus, Eq. (21) is transformed as

$$\frac{\partial v_{2a}}{\partial t} = \frac{1}{L^2}\frac{\partial}{\partial \xi}\left(D\frac{\partial v_{2a}}{\partial \xi}\right) - \frac{\partial v_{2c}}{\partial t} \tag{26}$$

The initial and boundary conditions are also transformed as shown below.

$$\text{At } t = 0,\quad 0 < \xi \le \frac{1}{2},\ v_{1a} = 1,\ v_{2a} = v_{2c} = 0 \tag{27}$$

$$\frac{1}{2} < \xi \le 1,\ v_{2a} = 1,\ v_{2c} = 0,\ v_{1a} = 0 \tag{28}$$

$$\text{At } \xi = 0 \text{ and } \xi = 1,\ \frac{\partial v_{1a}}{\partial \xi} = \frac{\partial v_{2a}}{\partial \xi} = 0 \tag{29}$$

2.4. Solution technique

The system of equations, Eq. (19) and Eqs. (26)–(29), are solved numerically by using the Crank–Nicholson method [59] to transform the differential equations to linear algebraic equations. The system of algebraic equations was re-written in a tri-diagonal form and solved using the Thomas algorithm [60]. The time step (Δt) in the simulation is 1 s. An adaptive spatial step (Δx) is used with $\Delta x = 1$ Å for distances within 300 nm of the interface and $\Delta x = 10$ Å for distances beyond 300 nm from the interface.

3. Experimental section

3.1. Materials and blend preparation

Linear low density of polyethylene (Exceed™ mLLDPE, Exxon Mobil) of molecular weight $\bar{M}_n = 32,400$ with a polydispersity index of 3.1 and isotactic polypropylene (Achieve™ 3854, Exxon Mobil) of molecular weight $\bar{M}_n = 47,500$ with a polydispersity index of 3.2 were used in this study. The melting temperature of PE and iPP, determined by differential scanning calorimetry (DSC) (Perkin Elmer DSC-7, Shelton, CT) with a scanning rate of 10 °C/min, are 117 and 153 °C, respectively. To make iPP/PE blends of different compositions, respective amounts of PE and iPP

were cooled by liquid nitrogen, and mixed and ground together in a freezer mill (SPEX, CertiPrep 6756, NJ).

3.2. Optical microscopy (OM)

A Nikon optical microscope (Eclipse ME 600L, JP) in the reflected mode was used to study the crystallization rate. Blends were pressed and melted by a Carver press (Wabash, IN) at 190 °C for 30 min to eliminate the crystals, and the thickness of the films is ~500 nm. The blend samples were then annealed at specific temperatures on a hot stage (Fryer, A200, IL), and the images of the spherulites were captured by a CCD camera (KP-M2, Hitachi, JP) as a function of time.

3.3. DSC

DSC was used to measure the degree of crystallinity of blends. Samples (~8 mg) were sealed in aluminum sample pans (Perkin Elmer DSC-7, Shelton, CT) and melted in the Carver press to eliminate the crystals prior to the measurement. An oven (Fisher Scientific, Isotemp 506G, Pittsburgh, PA) was used to anneal the blends to the crystallization equilibrium.

The calorimetric studies were performed in the DSC up to a temperature of 180 °C at a heating rate of 10 °C/min. The enthalpy changes (Δh) during the process can be analyzed by the area under the heat flow curve, and the degree of crystallinity was calculated as

$$X_e = \frac{\Delta h}{\Delta h_f} \tag{30}$$

here, X_e is the degree of crystallinity of the blends at crystallization equilibrium. The heat of fusion of iPP is 209 J/g [61].

3.4. Relationship between areal density of spherulites and degree of crystallinity

After the images were taken, the area occupied by the spherulites was analyzed by Image J (v1.31, National Institutes of Health, Bethesda, MD), and the volume fraction of the crystals was correlated to the area fraction of the crystals (A_c) using a dimensional factor, α.

$$\phi_c = \alpha A_c = \alpha \frac{\text{area occupied by crystals}}{\text{total area}} \tag{31}$$

In Eq. (31), α can be estimated by DSC. At equilibrium, the degree of crystallinity of iPP homopolymer measured by DSC is ~0.50, i.e. $\phi_c = 0.5$, and the crystals observed by OM are contained totally in the plane ($A_c = 1$). Thus, α can be calculated by Eq. (31), and is equal to 0.5. It is instructive to point out that α is related to an intrinsic property of the material, i.e. the equilibrium degree of crystallinity of iPP.

4. Results and discussion

4.1. Effect of blend composition and temperature on the crystallization rate constant

Fig. 1 shows the degree of crystallinity (from DSC) as a function of blend composition. The samples were annealed at 130 °C. This data shows that with increasing iPP composition in the blend, the degree of crystallinity increases linearly with a slope of ~0.5, indicating that only iPP crystallizes in the blend and α is a function of blend composition. In order to account for this behavior in the simulation, we add a constraint as shown in Eq. (32).

$$\frac{v_{2c}}{v_{2a} + v_{2c}} \le X_e \tag{32}$$

Eq. (32) implies that only iPP crystallizes in the blend, and the overall degree of crystallinity depends on the iPP blend composition. As the crystallization reaches equilibrium, the interfacial behavior only depends on the interdiffusion.

The isothermal crystallization kinetics was analyzed by using a modified form of Eq. (7) to obtain the Avrami exponent and rate constant (see previous section).

$$v_{2c} = \alpha[1 - \exp(-kt^m)] \tag{33}$$

To obtain the crystallization rate constant as a function of blend composition, the blend samples were annealed isothermally at 130 °C. At this temperature, the degree of supercooling is large, and crystallization is fast. Fig. 2 shows k as a function of blend composition. As the blend composition increases, k decreases. Using the experimental data, the parameter b in Eq. (10) can be extracted (see Table 1). In order to obtain the temperature dependence, isothermal crystallization studies of iPP homopolymer were performed at different temperatures (Fig. 3). Eq. (10) was used to analyze the data with the reference temperature, T_∞, being taken as T_m^o ($T_m^o = 186.2$ °C [62]). From this data,

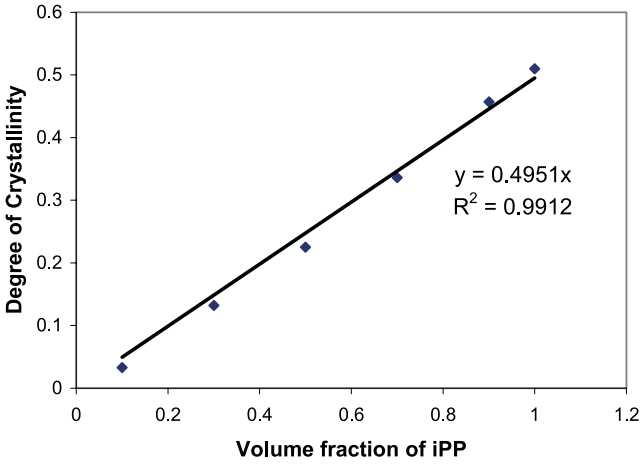

Fig. 1. Degree of crystallinity of iPP/PE blends annealed at 130 °C. The linear fit shows a slope of ~0.5.

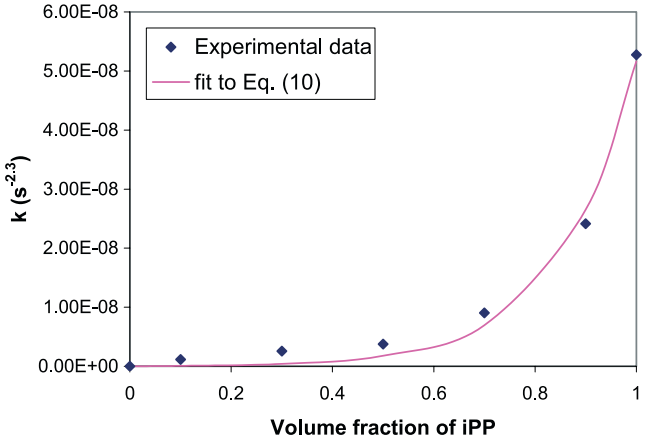

Fig. 2. The crystallization rate constant (k) as a function of iPP volume fraction under conditions of isothermal crystallization at 130 °C. The solid line is the curve fit by using Eq. (10).

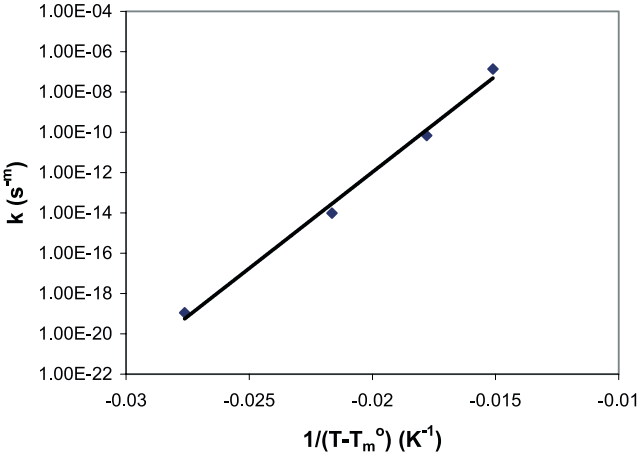

Fig. 3. The crystallization rate constant (k) of iPP homopolymer as a function of temperature. The linear fit shows the relationship between the rate constant and the degree of supercooling.

the temperature dependence of k can be quantified and the constants a and c can be extracted (see Table 1). Thus, the crystallization rate constant as a function of both temperature and iPP volume fraction is obtained.

The Avrami exponent (m) in this study is assumed to be independent of blend composition, which means m is only a function of temperature. Table 2 shows the Avrami exponents for different temperatures. In Table 2, m increases with increasing temperature, indicating that the mechanism of crystallization shifts from instantaneous nucleation to homogeneous nucleation [63].

4.2. Kinetics of interdiffusion

The simulations provide concentration profiles of amorphous iPP and PE and crystalline iPP as a function of position and time near the interface. The effect of polymer molecular weight, equilibrium degree of crystallinity, and temperature on the interfacial behavior was investigated.

Fig. 4 shows the change of volume fraction of the various components with time. The original polymer–polymer interface is located at 5000 Å. In the plots, we only show the region between 4800–5200 Å since there is no change outside this range. Fig. 4(a) and (b) show the profiles of amorphous PE and iPP respectively. We observe that PE and iPP interdiffuse with increasing time, and that PE diffuses faster than iPP (evidenced by the change of volume fraction on the iPP-rich and the PE-rich sides in Fig. 4(a)) due to the larger self-diffusion coefficient of PE, which favors the mutual diffusion coefficient on the PE-rich side.

Table 1
The parameters of the crystallization rate constant k (Eq. (10))

Constant	Value
a	1×10^{-7} (1/s^m)
b	6.7
c	18.1 (kJ/mol)

The volume fraction of crystalline iPP is shown in Fig. 4(c). For times below 1 h, there is no significant increase in the number of crystals. Crystals could be observed only after ~4 h of diffusion. The volume fraction of crystals is larger on the iPP side than at the interface because amorphous PE slows down the crystallization rate.

The effect of molecular weight on the volume fraction of iPP and PE at the interface is shown in Fig. 5. We assume that the crystallization is independent of molecular weight, but the diffusion coefficients, including D_{iPP} (Eq. (16)), D_{PE} (Eq. (17)) and mutual diffusion coefficient, D (Eq. (14)), are affected by molecular weight. Fig. 5(a) and (b) show that, after 12 h of interdiffusion, the interfacial width becomes broader as the molecular weight decreases because of larger self-diffusion coefficients. Besides, low molecular weight favors the entropic term (χ_s) in Eq. (11), which also enhances the mutual diffusion coefficient. As expected, the volume fraction of crystalline iPP in Fig. 5(c) is not a function of molecular weight.

The effect of X_e, which is the equilibrium degree of crystallinity of iPP, on the interfacial behavior was also investigated. Fig. 6(a) and (b) show the volume fraction of amorphous PE and iPP at the interface respectively for different values of X_e after 12 h of interdiffusion. The interfacial width slightly decreases with increasing X_e because the volume fraction of crystals at the interface is larger as X_e increases (Fig. 6(c)), which hinders the interdiffusion. In Fig. 6(c), the degree of crystallinity in the iPP-rich region also increases with X_e.

Table 2
Avrami exponent as a function of temperature

Temperature (°C)	m
120	2.0
130	2.3
140	2.5
150	2.9

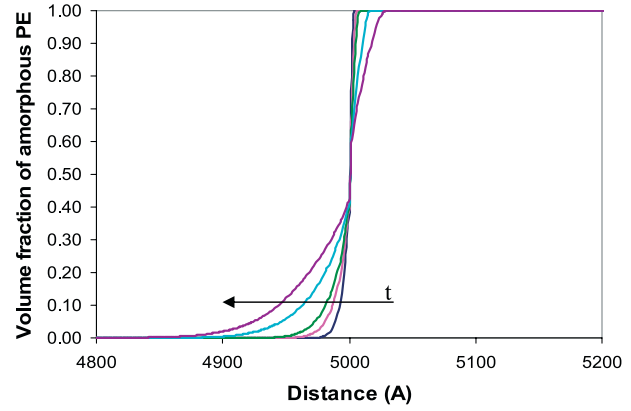

(a)

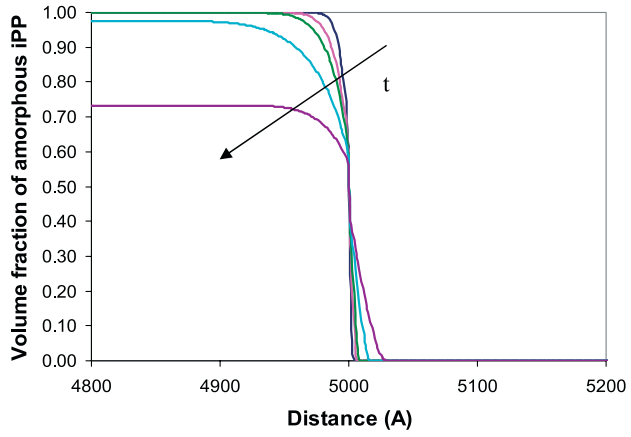

(b)

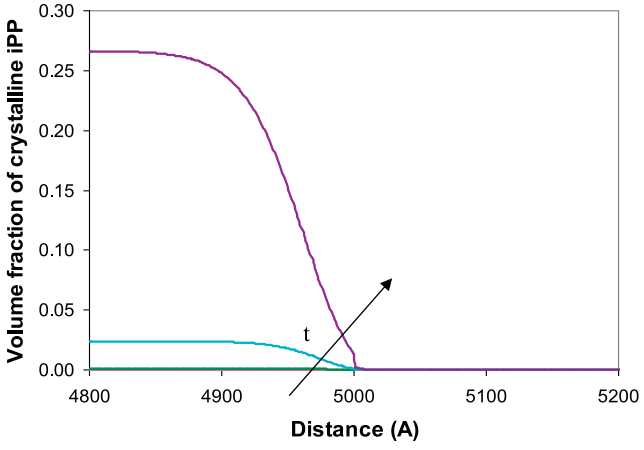

(c)

Fig. 4. Evolution of iPP/PE interfacial width with time ($T=140$ °C; $N_{iPP}=N_{PE}=1000$; $X_e=0.5$). (a) Volume fraction of amorphous PE (t increases from right to left: 10 min; 30 min; 1 h; 4 h; 12 h). (b) Volume fraction of amorphous iPP (t increases from right to left: 10 min; 30 min; 1 h; 4 h; 12 h). (c) Volume fraction of crystalline iPP (t increases from left to right: 1 h; 4 h; 12 h).

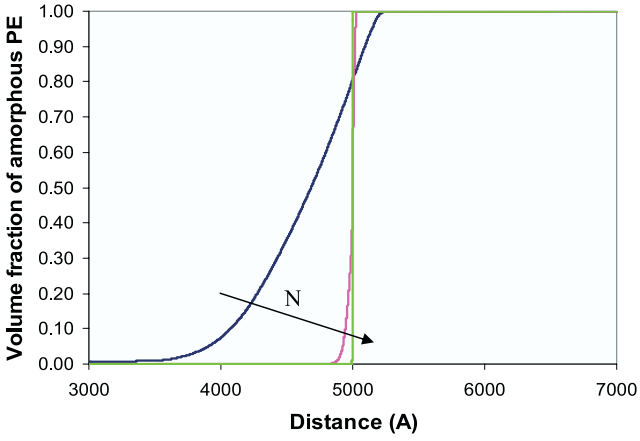

(a)

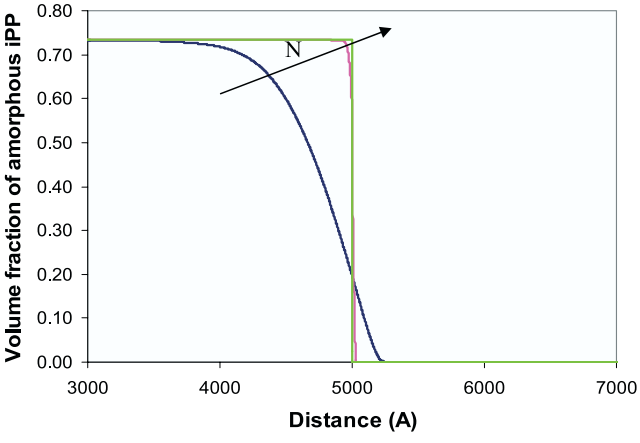

(b)

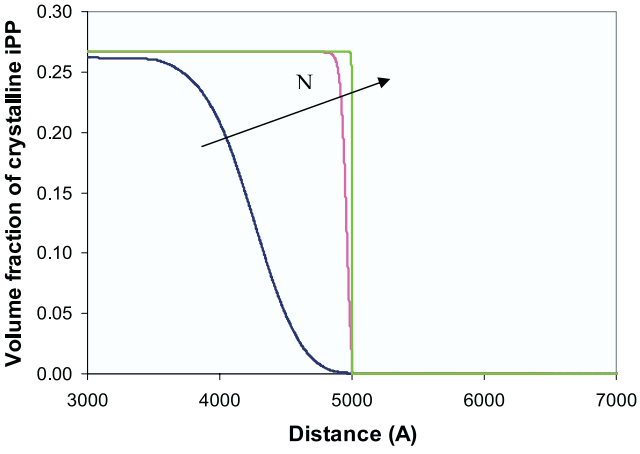

(c)

Fig. 5. Effect of molecular weight on iPP/PE interfacial behavior ($t=12$ h; $T=140$ °C; $X_e=0.5$). (a) Volume fraction of amorphous PE. (b) Volume fraction of amorphous iPP. (c) Volume fraction of crystalline iPP. In these figures, N increases from left to right: 100; 1000; 10000.

The interfacial behavior as a function of temperature is shown in Fig. 7. As the temperature increases, the mutual diffusion coefficients also increase, which increases the interfacial width. This effect can be observed in Fig. 7(a). As the temperature increases from 120–160 °C, a higher number of PE chains diffuse into the iPP-rich region after 8 h of interdiffusion. It is instructive to point out that at

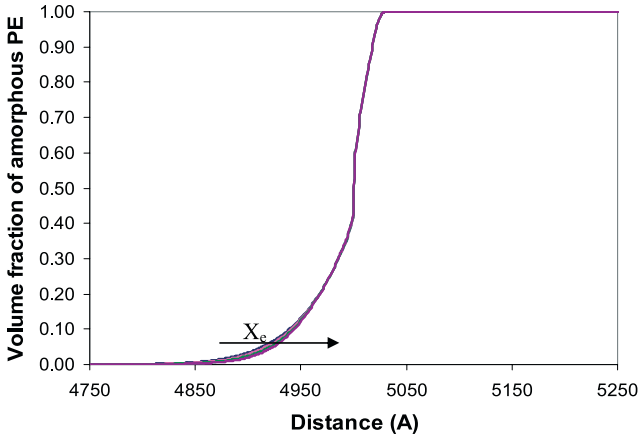

(a)

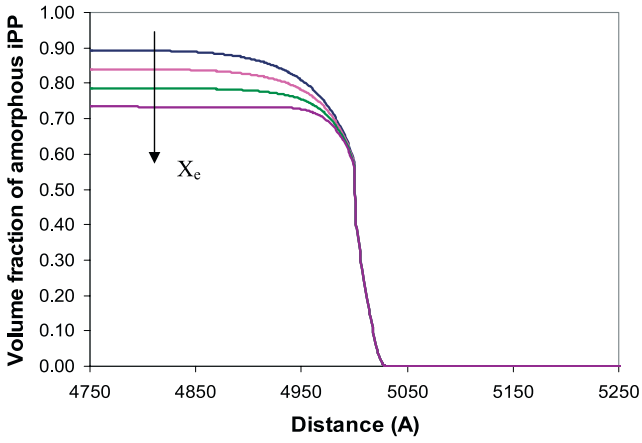

(b)

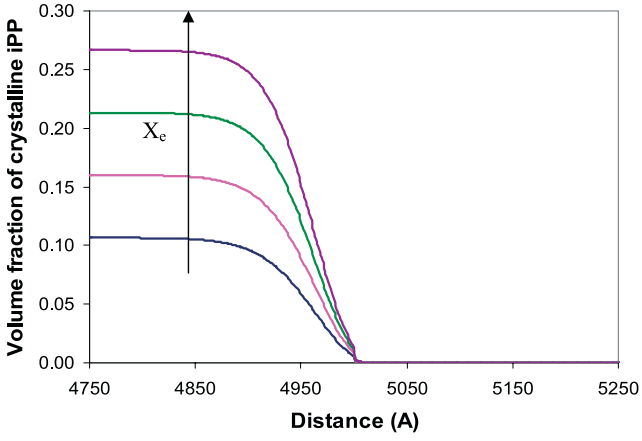

(c)

Fig. 6. Effect of X_e on iPP/PE interfacial behavior ($t=12$ h; $T=140$ °C; $N_{iPP}=N_{PE}=1000$). (a) Volume fraction of amorphous PE (X_e increases from left to right: 0.2; 0.3; 0.4; 0.5; 0.6). (b) Volume fraction of amorphous iPP (X_e increases from top to bottom: 0.2; 0.3; 0.4; 0.5; 0.6). (c) Volume fraction of crystalline iPP (X_e increases from bottom to top: 0.2; 0.3; 0.4; 0.5; 0.6).

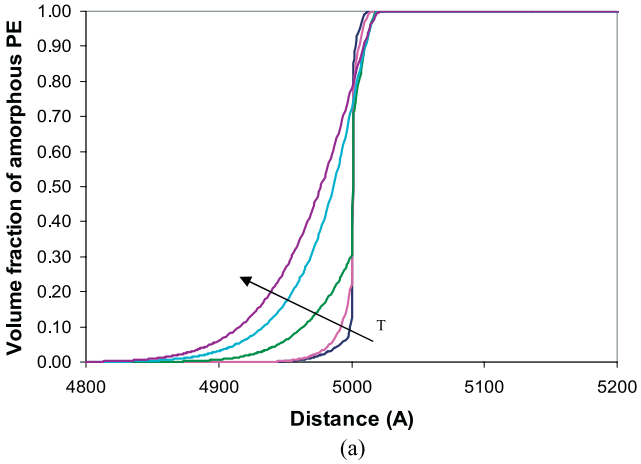

(a)

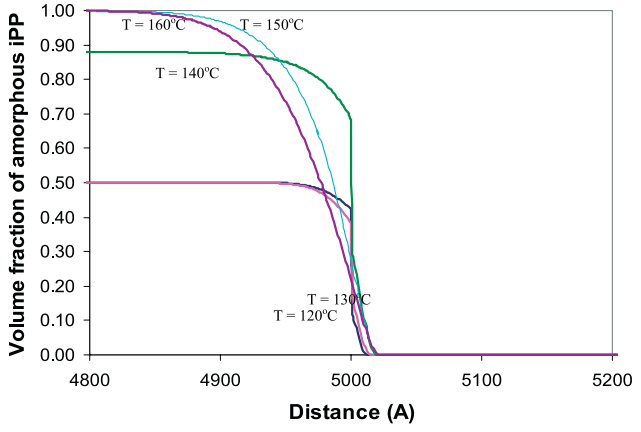

(b)

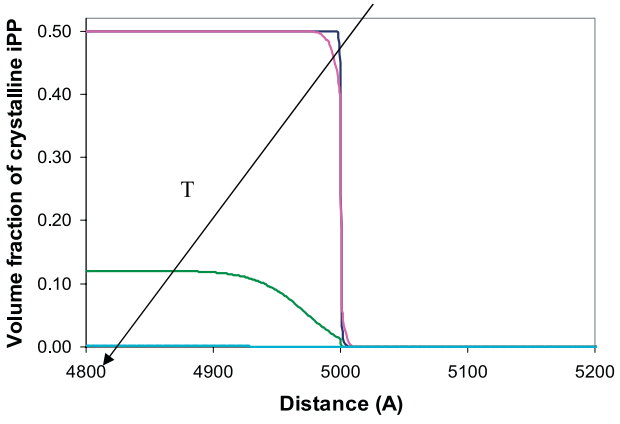

(c)

Fig. 7. Effect of temperature on interfacial behavior ($t=8$ h; $N_{PE}=1157$; $N_{iPP}=1131$; $X_e=0.5$). (a) Volume fraction of amorphous PE (T increases from right to left: 120; 130; 140; 150; and 160 °C). (b) Volume fraction of amorphous iPP. (c) Volume fraction of crystalline iPP (T increases from top to bottom: 120; 130; 140; 150; and 160 °C).

160 °C, both polymers are molten, and the system is amorphous. Fig. 7(b) shows the volume fraction of amorphous iPP as a function of temperature. Below 140 °C, the density profiles at the interface are very steep, whereas above 150 °C, the profiles are broad and smooth. This is because the crystallization is fast at low temperatures, which hinders the interdiffusion, and narrows the interfacial width. This result can also be gleaned from the

profile of the volume fraction of crystalline iPP shown in Fig. 7(c). At 150 °C, the crystallization is very slow (due to the small degree of supercooling), and the crystals are not observed even after 8 h. At this condition, interdiffusion dominates crystallization, and there is no barrier to interdiffusion (since the system is miscible). Therefore, the behavior at the interface is similar to that at an amorphous polymer interface (see the profiles at 150 and 160 °C in Fig. 7(b)). Below 140 °C, crystallization rate increases with the degree of supercooling, and the crystals grow fast. Thus, at low temperatures, the crystallization dominates interdiffusion, and hinders the interdiffusion. These effects are quantitatively captured by the model.

The interfacial width as a function of temperature can be calculated from the volume fraction profiles by using the following expression [64].

$$v_a(x) = \frac{1}{2}\left(1 + \tanh\frac{x}{l}\right) \tag{34}$$

here, l is one-half of the total interfacial width. We use the profiles of the volume fraction of amorphous PE to fit the hyperbolic tangent equation and extract the interfacial width ($2\,l$). Table 3 shows the interfacial width obtained from Eq. (34) as a function of temperature. The theoretical interfacial width can be estimated from Eq. (5) [26]. The value of χ_c in Eq. (5) is 1.75×10^{-3}, and c can be calculated from Eq. (35) [23].

$$c_s = \left(\frac{c_{iPP}^2 + c_{PE}^2}{2}\right)^{1/2} \tag{35}$$

here, c_{iPP} and c_{PE} are the segment lengths of iPP and PE, and taken as 6.50 and 2.55 Å, respectively [1]. The interfacial width calculated by using Eq. (5) is slightly larger than the interfacial width predicted by the kinetic model because Eq. (5) was derived for amorphous polymer interfaces. The interfacial behavior of semicrystalline polymers depends on the competition between crystallization and interdiffusion [29]. At low temperatures, crystallization is fast, and hinders the interdiffusion, which leads to narrow interfacial widths.

Table 3 also shows the comparison between the interfacial width obtained from Eq. (34) and the experimental interfacial widths (from previous TEM studies [29]). The interfacial widths measured by TEM are much larger since the polymers are polydisperse. As shown before by several researchers [29,65], during annealing, small molecules accumulate at the interface and broaden the interfacial width. Additional factors that contribute to smaller interfacial widths from theory include concentration fluctuations, chain end effects, distorted chain conformation, and initial roughness.

As evidenced from the comparison with experiment, the model has limitations. However, it correctly predicts trends with respect to temperature, polymer molecular weight, and degree of crystallinity. This model can be generalized and extended to different semicrystalline polymer systems. By using the Avrami equation, the kinetics of crystallization can be quantified and incorporated into the model to study the effect of polymer molecular weight, equilibrium degree of crystallinity, and annealing conditions on the interfacial behavior. This provides a quantitative understanding of the competition between interdiffusion and crystallization and its effect on interfacial behavior. Such an understanding of interfacial phenomena is crucial because it is related to the mechanical properties of the interface [16–18,66], which in turn affects the performance of the material. The model also captures the role of processing conditions on interfacial properties, which has important consequences for co-extruded materials, blends, and composites.

5. Conclusions

A kinetic model has been developed, which considers both interdiffusion and crystallization, to predict the interfacial behavior of semicrystalline polymer systems. The interdiffusion coefficient is a function of blend composition, temperature, and molecular weight and is obtained from the fast mode theory, and the temperature and blend composition dependence of the crystallization rate, which is measured by optical microscopy and DSC, is based on the Avrami equation. This model reveals that the presence of crystallites near the interface significantly affects the interfacial behavior, particularly interdiffusion. Thus, long processing times, small molecular weights, low equilibrium degrees of crystallinity, and high annealing temperatures favor the evolution of the interfacial width because at those conditions interdiffusion dominates crystallization. The interfacial width extracted from the concentration profiles is qualitatively consistent with that measured by TEM. The model provides new insights on the various phenomena that control interfacial behavior in

Table 3
Comparison of interfacial widths obtained from the kinetic model and previous TEM studies [29]

Temperature (°C)	Interfacial width obtained from the kinetic model (nm)	Interfacial width measured by TEM (nm)
120	2.8	~0.0
130	3.6	17.6
140	8.0	35.6
150	9.0	42.5
160	11.2	49.0

semicrystalline polymer systems and can be used for rational design of such interfaces.

Acknowledgements

We appreciate financial support from the USDOE Ames Laboratory (Contract No. W-7405-ENG-82).

References

[1] Wool RP. Polymer interfaces: structure and strength. Cincinnati, OH: Hanser/Gardner; 1995.
[2] Kramer EJ, Green P, Palmstrom CJ. Polymer 1984;25:473–80.
[3] Green PF, Palmstrom CJ, Mayer JW, Kramer EJ. Macromolecules 1985;18:501–7.
[4] Brochard F, de Gennes PG. Europhys Lett 1986;1(5):221–4.
[5] de Gennes PG. Adv Colloid Interf Sci 1987;27:189–209.
[6] Composto RJ, Kramer EJ, White DM. Macromolecules 1988;21: 2580–8.
[7] Jordan EA, Ball RC, Donald AM, Fetters LJ, Jones RAL, Klein J. Macromolecules 1988;21:235–9.
[8] Rafailovich MH, Sokolov J, Jones RAL, Krausch G, Klein J, Mills R. Europhys Lett 1988;5(7):657–62.
[9] Jabbari E, Peppas NA. Polym Int 1995;38:65–9.
[10] Guckenbiehl B, Stamm M, Springer T. Physica B 1994;198:127–30.
[11] Agrawal G, Wool RP, Dozier WD, Felcher GP, Zhou J, Pispas S, Mays JW, Russell TP. J Polym Sci Polym Phys Ed 1996;34:2919–40.
[12] Bucknall DG, Butler SA, Hermes HE, Higgins JS. Physica B 1998; 241–243:1071–3.
[13] Bucknall DG, Butler SA, Higgins JS. J Phys Chem Solids 1999;60: 1273–7.
[14] Yeung C, Shi AC. Macromolecules 1999;32:3637–42.
[15] Jablonski EL, Gorga RE, Narasimhan B. Polymer 2002;44(3):729–41.
[16] Schnell R, Stamm M, Creton C. Macromolecules 1998;31:2284–92.
[17] Schnell R, Stamm M, Creton C. Macromolecules 1999;32:3420–5.
[18] Gorga RE, Narasimhan B. J Polym Sci Polym Phys Ed 2002;40: 2292–302.
[19] Zhang H, Wool RP. Macromolecules 1989;22:3018–21.
[20] de Gennes PG. J Chem Phys 1971;55:572.
[21] Helfand E, Tagami Y. Polym Lett 1971;9:741–6.
[22] Helfand E, Tagami Y. J Chem Phys 1972;56:3592–601.
[23] Helfand E, Sapse AM. J Chem Phys 1975;62(4):1327–31.
[24] Anastasiadis SH, Gancarz I, Koberstein JT. Macromolecules 1988;21: 2980–7.
[25] Broseta D, Fredrickson GH, Helfand E, Leibler L. Macromolecules 1990;23:132–9.
[26] Chaturvedi UK, Steiner U, Zak O, Krausch G, Klein J. Phys Rev Lett 1989;63(6):616–9.
[27] Stamm M, Schubert DW. Annu Rev Mater Sci 1995;25:325–56.
[28] Yuan BL, Wool RP. Polym Eng Sci 1990;30(22):1454–65.
[29] Lo CT, Laabs FC, Narasimhan B. J Polym Sci Polym Phys Ed 2004; 42:2667–79.
[30] Bartczak Z, Galeski A. Polymer 1986;27(4):537–43.
[31] Bartczak Z, Galeski A. Polymer 1986;27(4):544–8.
[32] Kumar SK, Yoon DY. Macromolecules 1989;22:3458–65.
[33] Kumar SK, Yoon DY. Macromolecules 1989;22:4098–101.
[34] Kumar SK, Yoon DY. Macromolecules 1991;24:5414–20.
[35] Avrami M. J Chem Phys 1939;7:1103–12.
[36] Avrami M. J Chem Phys 1940;8:212–24.
[37] Avrami M. J Chem Phys 1941;9:177–84.
[38] Shanks RA, Li J, Yu L. Polymer 2000;41:2133–9.
[39] Li J, Shanks RA, Long Y. Polymer 2001;42:1941–51.
[40] Li J, Shanks RA, Olley RH, Greenway GR. Polymer 2001;42: 7685–94.
[41] Lauritzen JI, Hoffman JD. J Res Nat Bur Std 1960;64A:73–101.
[42] Hoffman JD. Polymer 1982;23:656–70.
[43] Hoffman JD. Polymer 1983;24:3–26.
[44] Flory PJ. Principles of polymer chemistry. Ithaca, NY: Cornell University Press; 1953.
[45] Binder K. J Chem Phys 1983;79(12):6387–409.
[46] Brochard F, Jouffroy J, Levinson P. Macromolecules 1983;16: 1638–41.
[47] Jabbari E, Peppas NA. Macromolecules 1993;26(9):2175–86.
[48] Jabbari E, Peppas NA. Polymer 1995;36(3):575–86.
[49] Meier H, Strobl GR. Macromolecules 1987;20:649–54.
[50] Akcasu AZ. Polym Mater Sci Eng 1994;71:771–2.
[51] Akcasu AZ, Naegele G, Klein R. Macromolecules 1995;28(19): 6680–3.
[52] Akcasu AZ. Macromol Theory Simul 1997;6(4):679–702.
[53] Alfonso GC, Russell TP. Macromolecules 1986;19:1143–52.
[54] Tirrell M. Rubber Chem Technol 1984;57:523–56.
[55] Gell CB, Graessley WW, Fetters LJ. J Polym Sci Polym Phys Ed 1997;35:1933–42.
[56] McCall DW, Douglass DC, Anderson EWJ. Chem Phys 1959;30(3): 771.
[57] Eckstein A, Suhm J, Friedrich C, Maier RD, Sassmannshausen J, Bochmann M. Macromolecules 1998;31:1335–40.
[58] Lo CT, Seifert S, Thiyagarajan P, Narasimhan B. Polymer 2004;45: 3671–9.
[59] Zill DG, Cullen MR. Advanced engineering mathematics. 2nd ed. Sudbury, MA: Jones and Bartlett Publications; 2000.
[60] Hoffman JD. Numerical methods for engineers and scientists. New York: McGraw Hill; 1992.
[61] Brandrup J, Immergut EH. Polymer handbook. 3rd ed. New York: Wiley; 1989.
[62] Yamada K, Hikosaka M, Toda A, Yamazaki S, Tagashira K. Macromolecules 2003;36:4790–801.
[63] Sperling LH. Introduction to physical polymer science. 3rd ed. New York: Wiley; 2001.
[64] Cahn JW, Hilliard JE. J Chem Phys 1958;28:258–67.
[65] Chaffin KA, Knutsen JS, Brant P, Bates FS. Science 2000;288(23): 2187–90.
[66] Foster KL, Wool RP. Macromolecules 1991;24(6):1397–403.